Feasibility of simultaneous intracranial EEG-fMRI: a safety study

Authors: David W Carmichael[1] PhD, John S Thornton[2] PhD, Roman Rodionov[1] PhD, Rachel Thornton[1] MRCP, Andrew W McEvoy[3] MD, Roger J Ordidge PhD[5], Philip J Allen[6], Louis Lemieux[1] PhD

1 Department of Clinical and Experimental Epilepsy, UCL Institute of Neurology, London, UK

2 Lysholm Department of Neuroradiology, National Hospital for Neurology and Neurosurgery, London, UK

3 Victor Horsley Department of Neurosurgery, National Hospital for Neurology and Neurosurgery, London, UK

4 Wellcome Trust Centre for Neuroimaging, UCL Institute of Neurology, London, UK

5 Department of Medical Physics and Bioengineering, UCL, London, UK

6 Department of Clinical Neurophysiology, National Hospital for Neurology and Neurosurgery, London, UK

Corresponding Author: David Carmichael
Correspondance Address: Advanced Magnetic Resonance Imaging Group
UCL Institute of Neurology
12 Queen Square
London WC1N 3AR
Tel +44 (0)20 76762006
Fax +44 (0)20 76762005
email d.carmichael@ion.ucl.ac.uk

Keywords: Safety, EEG, fMRI, intracranial EEG, Epilepsy, simultaneous intracranial EEG-fMRI

Running head: safety of intracranial EEG-fMRI

Abstract

In epilepsy patients who have electrodes implanted in their brains as part of their pre-surgical assessment, simultaneous intracranial EEG and fMRI (icEEG-fMRI) may provide important localising information and improve understanding of the underlying neuropathology. However, patient safety during icEEG-fMRI has not been addressed.

Here the potential health hazards associated with icEEG-fMRI were evaluated theoretically and the main risks identified as: mechanical forces on electrodes from transient magnetic effects, tissue heating due to interaction with the pulsed RF fields and tissue stimulation due to interactions with the switched magnetic gradient fields. These potential hazards were examined experimentally in-vitro on a Siemens 3 T Trio, 1.5 T Avanto and a GE 3 T Signa Excite scanner using a Brain Products MR compatible EEG system.

No electrode flexion was observed. Temperature measurements demonstrated that heating well above guideline limits can occur. However heating could be kept within safe limits (<1.0°C) by using a head transmit RF coil, ensuring EEG cable placement to exit the RF coil along its central z-axis, using specific EEG cable lengths and limiting MRI sequence specific absorption rates (SARs). We found that the risk of tissue damage due to RF-induced heating is low provided implant and scanner specific SAR limits are observed with a safety margin used to account for uncertainties (e.g. in scanner-reported SAR). The observed scanner gradient-switching induced current (0.08mA) and charge density (0.2μC/cm^2) were well within safety limits (0.5mA and 30μC/cm^2, respectively).

Introduction

In cases of drug-resistant focal epilepsy, surgery to remove the tissue involved in seizure onset can be an effective treatment [1]. Selection of the surgical target area is commonly based on the combined assessment of MR imaging and video-scalp electroencephalography (EEG) telemetry. The main aim of pre-surgical evaluation is to gather converging evidence that there is a single epileptic focus. In some cases, non-invasive pre-surgical investigations do not lead to a clear localisation and the implantation of intracranial electrodes may be considered [2]. A combination of brain indwelling needle-shaped electrodes or subdural electrode grids or strips may be placed at locations chosen to allow the testing of one or a number of alternative hypotheses for the spatial location of the origin of the seizures. Intracranial EEG (icEEG) recording is generally considered the gold standard for localising epileptic activity. However, icEEG has its own limitations including low spatial resolution (typically $1cm^3$ [2]) and restricted brain coverage due to the relatively small volume of sensitivity of the individual contacts and the difficulty and risks of implanting multiple electrodes [3], leaving the possibility that the pathological source position, extent or structure is not clear. These limitations could potentially be mitigated if icEEG recording were used in combination with functional MRI (fMRI). Indeed, despite its own limitations scalp EEG has previously been successfully combined with fMRI in study patients with epilepsy, providing unique new information on the haemodynamic correlates of paroxysmal discharges in a good proportion of cases studied to date [4-8]. Importantly, these include brain areas thought to be primarily responsible for the generation of interictal and ictal epileptic discharges visible on scalp EEG recordings [5,7,9,10]. However, EEG-fMRI studies in epilepsy have raised a number of important questions, for example; 1) is normal neurovascular coupling maintained, as in cognitive fMRI experiments [12-16]? 2) What are the implications of using scalp EEG, with its limited sensitivity to deep sources, to define the events and baseline? [11,5]; 3) What is the interpretation of positive and negative BOLD changes in relation to the

same discharges? [6]; 4) Can clinically relevant information be derived from the fMRI signal when no pathological EEG events are recorded on the scalp?

Even in cases where invasive recordings are available allowing comparison with the scalp EEG-fMRI findings, these are often performed days, weeks or even months apart and the patient may therefore be in a different state rendering direct comparison with fMRI findings difficult. Simultaneously acquired icEEG-fMRI could help address this problem and provide insights into some of the questions highlighted above thus improving our understanding of the haemodynamic changes linked to epileptic activity. This could have a beneficial impact on our ability to model scalp EEG-fMRI and hence increase the utility of the less invasive measurements.

We have identified 4 main acute health risks associated with the presence of intracranial electrodes during MRI:

1. RF-induced heating of the tissue surrounding the electrodes;
2. Switching magnetic gradient fields inducing currents in the electrode circuit;
3. Induced currents caused by movement of the head, or independent motion of the electrode leads, through the static magnetic field;
4. Forces or torques on the implants due to permanent or transient magnetic effects.

Combinations of these have been previously studied in the context of scalp EEG-fMRI [18] and active deep brain stimulation (DBS) during MRI [19-24]. Depending on their frequency and amplitude, excessive currents in tissue may cause electro-motive forces, electrolysis, depolarisation and stimulation, burning, coagulation, and vaporisation which can all lead to cell damage and ultimately cell death [25-27].

In this paper we examine each risk from a theoretical perspective and then present experimental assessments of those risks found to pose a significant concern on theoretical grounds. We then interpret our results with respect to safe limits derived from both medical devices and MRI safety literature to determine those circumstances under which simultaneous icEEG-fMRI may be safe. To our

knowledge this study represents the first systematic attempt to address the safety of performing simultaneous intracranial EEG-fMRI in humans.

Theory

In this section the mechanisms of electromagnetic interaction between conducting implants and the MRI system are reviewed and, based on worst-case estimates, existing safety guidelines and other relevant literature, the need or otherwise for empirical safety assessments are identified.

The potential for tissue damage (risks #1-3 above) is related to the electric field $\vec{E}$ which in turn may be expressed in terms of the electric potential field (φ) and the vector potential ($\vec{A}$).

$$\vec{E} = -\Delta\phi - d\vec{A}/dt \qquad [1]$$

In a conducting medium, the resulting induced currents obey Ohm's law:

$$J = \sigma \cdot \vec{E} \qquad [2]$$

Where J is the current density and σ the electrical conductivity. For risk #4, the Lorentz force on the implant depends on the induced currents, the length of the wire and its orientation relative to the scanner's static magnetic field in the absence of any permanently magnetic electrode components.

Induced voltage due to time-varying magnetic fields

Using the integral form of Eq. [1], we can express the induced electromotance (*V*) created in a closed circuit (i.e. a 'low impedance loop' in the context of this work), with a given area (A) exposed to a time-varying magnetic field ($\vec{B}$), as the Faraday induction law:

$$V = -\frac{d}{dt}\oiint \vec{B}(t) \bullet dA(t) \qquad [3]$$

Both switching magnetic field gradients and RF pulses produce time varying magnetic fields and so induce a voltage in a circuit, such as the subject's body with conducting objects in contact with it, according to equation (3). Conversely, movement of the body through the static field can also result in an induced voltage.

Theoretical estimation of the maximum effect size due to gradient switching

For switched magnetic field gradients the maximum value of voltage induced in an implanted circuit can be estimated given the maximum area perpendicular to the magnetic field made by any loop comprising the electrodes, cables and amplifiers, and the gradient slew rate. This voltage is the product of loop area (A), gradient slew rate (S) and position from gradient centre (*z*):

$$V = S_{\max} Az \qquad [4]$$

A good worst case estimate for a practical icEEG experimental arrangement may be represented by a conducting loop placed 1m from the magnet isocentre, and gradients of strength 69.3mT/m (40mT/m summed over xyz) that can be switched in 200μs (Siemens TQ gradients - see methods for details), giving S_{max}=346T/m/s. The largest likely loop area formed by 2 electrode-contact and lead pairs (each ~40cm length) connected in a circular fashion would be 0.05m^2. This worst-case scenario would result in an induced voltage of approximately 17V. For echo planar imaging (EPI), we can estimate the resulting rms voltage if we assume 50 slices are obtained with 96 gradient switches per slice in each TR of 3s; this equates to 17V with a duty cycle of 1/3, resulting in V_{rms} = ~6V. Thus for a conservative estimate of tissue impedance, 500Ω, [28] the corresponding rms current is 12mA. In practice such a low-impedance closed loop at gradient switching frequencies (~1kHz) will only be formed if a fault occurs at the amplifier, the electrode leads (termed tails) have a short-circuit, or the tail terminations are in electrical contact. This corresponds to a single-fault condition as defined in the electrical safety standard for medical devices, for which the maximum allowed rms current is 0.5mA [29], which this worst case induced current substantially exceeds.

The induced surface charge density can be calculated by dividing the product of the voltage and pulse width by the product of the impedance and electrode surface area

[28]. As an assessment of risk, using the estimated worst case induced voltage of 17V and assuming an approximately square pulse-shape, gradient switching time of 200μs, electrode contact-area 0.07cm^2, and tissue impedance 500Ω, the estimated surface-charge density is 97μC/cm^2, exceeding the limit (30μC/cm^2) necessary to cause stimulation and tissue damage. Hence, an experimental investigation of gradient-induced voltages is justified.

Theoretical estimation of the maximum effect due to movement in the static field (B_0)

Voltages may also be induced in the EEG-patient circuit by movement of the patient through the static magnetic field (B_0) (e.g. when being moved into the magnet isocentre for scanning)[1]. If this were to occur at a speed of 1m/s, which is much faster than in normal circumstances, in a stray-field gradient of 3T/m, S_{max}=3T/m/s. Assuming, as above, the loop area perpendicular to the changing gradient to be 0.05m^2 this relative motion will induce a voltage of 0.15V (using Eq. [2]) causing a current of 0.3mA (assuming again 500Ω tissue impedance). Hence low-frequency induced voltages due to relative motion in the field are unlikely to exceed the guideline limit (0.5mA see appendix.A). This safety condition can easily be ensured by requiring that the patient is moved slowly when approaching the scanner table and that a slow bed-speed is used to move the patient into the scanning position.

Estimation of maximum effect due to exposure to RF (B1) field

At RF frequencies the magnitude of B1-induced voltages are less amenable to simple calculation and depend upon more complex factors than simply loop area. Indeed, single straight wires not forming a loop can be subject to large RF-currents because both the implant and the tissue exhibit inductive properties and form circuits that can be resonant. Even for relatively simple arrangements of straight wires,

[1] We assume that the amount of motion during the scanning process will be much smaller due to the use of head restraint.

complicated behaviour can result from differences in factors such as lead length [30]. Furthermore, multiple electrodes and leads can form coupled circuits resulting in greater induced voltages, as inferred in heating measurements [31-32] which are difficult to predict *a priori*. Hence empirical investigations are required at RF frequencies. In addition the precise location of a conductive implant within the non-uniform RF field can be critical [33] hence measurements testing a range of lengths and locations are needed. In practice, it is difficult to directly and accurately measure current density directly, or voltage at RF frequencies, because the signals must be measured from the electrode contacts themselves and the measurement circuit will often interact with the investigated arrangement (i.e. the implant and the RF coil) changing its electrical properties. Additionally, the electrode-impedance is highly dependant on tissue and electrode properties, further decreasing experimental accuracy. Since the dominant B1-related safety issue is tissue heating, we investigated the important consequence of RF-effects directly by thermometry.

Mechanical forces on the implant

The platinum electrodes and cables used in our centre are devoid of ferromagnetic materials avoiding forces resulting from static placement in the B_0 magnetic field. However, transient currents induced in these conductors might be subject to forces causing their movement or distortion. We therefore performed simple experiments to investigate this risk.

Materials and Methods

Experiments were performed using a tissue-simulating test object with a range of icEEG electrode and lead arrangements in a 1.5 T and two different 3 T MRI systems during scanning. These experiments were intended to investigate RF-related temperature increases and the effects upon them of varying the EEG electrode cable's position, termination and length. In addition, induced voltages in the EEG circuit associated with gradient field switching, and electrode-lead displacements were investigated.

Experimental setup

A Perspex phantom, similar to one described previously [19,23], which broadly follows the ASTM standard for testing passive implants [34] was formed with a shape and dimensions approximating those of an adult human torso (Figure 1). This was filled to a depth of approximately 10cm with a semi-liquid gel comprising distilled water, poly-acrylic acid partial sodium salt (Aldrich Chemical) (8g/litre) and sodium chloride (0.70 g/litre) with electrical (conductivity of 0.26 Sm^{-1}) and thermal characteristics (limited convection) similar to those of human tissue [34,35].

The intracranial electrodes tested were of a type commonly used at our (and many other institutions) for icEEG monitoring in epilepsy patients. The depth electrodes (Ad-Tech, Racine, WI) consist of platinum contacts of length 2.3mm and radius 1mm, with nickel-chromium wires in polyurethane tubing leading to nickel-chromium tail contacts. Three depth electrodes of 2 designs were used: 1 SD-8PX (8 electrode contacts with 10mm spacing, total length 380mm), 2 SD-6PX (6 electrode contacts with 10mm spacing, total length 370mm). One grid and one strip electrode array (also Ad-Tech, Racine, WI) were investigated: 1 T-WS-6PX strip (6-contact electrode with 10mm spacing, total length 445mm) and 1 T-WS-48PX grid (6x8 contacts with 10mm spacing, and tails, total length 455mm). Each has contacts consisting of 4mm diameter platinum-iridium disks (2.3mm exposed) imbedded within a silicon sheet

with stainless steel (316) wires and nickel-chromium tail contacts contained within polyurethane tubing.

For experiments in measurement set A (see below), 3 depth electrodes, 1 subdural grid and 1 strip electrode were positioned within the “head” region of the phantom (Figure 1). The depth electrodes were inserted along the left-right axis and perpendicularly to the sagittal plane, 2 on the left hand side (LHS) (1 x 8 contacts, 1 x 6 contacts) and 1 on the right hand side (RHS) (1 x 6 contacts). This simulated implants targeting the left hippocampus and amygdala with contra-lateral control. The electrodes’ leads were run along the phantom wall (within the gel) for 40mm before exiting the phantom to simulate surgical implantation with electrode-leads tunnelled under the skin away from the cranial window to avoid infection. The lead lengths inside/outside the phantom for the grid electrode were 155/300mm, for the strip electrode 95/350mm, for the RHS depth electrode 120/250mm, for the LHS 6 contact electrode 105/265mm, for the LHS 8 contact electrode 115/265mm. The subdural grid and strip electrodes were positioned so as to simulate implants recording from the cortical surface. In this way, surgically realistic implant placement positions were used with the total number of electrodes and electrode contacts being the maximum likely according to current clinical practice in our centre. For experiments involving the MRI compatible EEG amplifier (measurement sets B and C; see below) the strip and second RHS depth electrodes were removed (electrodes indicated with dashed lines in Figure 1) to reduce the number of recording sites / electrode contacts below the number of amplifier channels (64).

Experiment set A) The effect of cable position within the scanner bore on heating was investigated. Cables were attached to the electrode tails (Tech-Attach Cables, 1x L-DC-64DIN, 1x L-DC-6DIN, 1x L-DC-8DIN, Ad-Tech, Racine WI) using their respective connector blocks (Tech-Attach disposable connector blocks, models DC-8X and DC-6x). These are effectively ribbon cables with specialist connectors which connect to the electrode tails at one end and have 1.5mm touch proof terminations at

the opposite end. The cables used had a total length of 120cm and were placed in different positions within the scanner bore to establish the sensitivity of the induced heating to cable position. Firstly, the cables were positioned along the z-axis for 30cm before being run along the bottom of the scanner bore (Figure 2a). Secondly, the cables were run back past the body (Figure 2b); the sensitivity of temperature increases to the exact cable position in this configuration was tested again with the cables deliberately placed close to the RF coil and its internal components. The electrodes or cables were terminated in either a short or open circuit to model the 2 possible extremes of circuit impedance. The short-circuit condition was achieved by emersion of the cable terminations in EEG electrode gel (Elefix, Nihon Kohden, Tokyo, Japan).

Experiment set B) The effect of variations in amplifier input impedance value on electrode heating was investigated by testing 3 different cable terminations. The cables were connected to an MRI compatible 64 channel EEG recording system (BrainAmp MR plus, Brain Products, www.brainproducts.com) via a 64 channel touch-proof input box (Brain Products) and two short 30cm ribbon cables which were connected into two 32 channel amplifiers (Figure 3). Measurements were repeated with either an open circuit (30cm ribbon cable not connected to amplifier) or a short circuit (no amplifier and one 32 channel ribbon connecting the first 32 channels to the second 32 channels at the output of the 64x input box) to attempt to model the 2 possible extremes of cable-termination impedance and to asses possible differences in heating caused by a fault condition.

Experiment set C) The cables between the implants and amplifier were varied in length by modifying one Tech-Attach Cable (Ad-Tech, L-DC-64DIN, 120cm) so that the total cable length could be altered by inserting different length ribbon cable middle sections. Inserts of length 20, 40, 60 and 90cm were added individually to the two 30cm end sections (the original cable length being 120cm equivalent to using the

the 60cm insert). These results were compared to those from a new unmodified Tech-Attach Cable (Ad-Tech, 1x L-DC-48DIN, 2x L-DC-8DIN, length 180cm).

Temperature measurements

Continuous temperature measurements were made simultaneously from 4 positions using an MRI-compatible fluoroptic thermometer (Model 3100, Luxtron Corporation, Santa Clara, CA, USA; accuracy ±0.1ºC; SMM probes). The electrode tips are generally considered the locations most likely to demonstrate the largest temperature change [36,37]. To confirm this we performed a number of pilot experiments placing the sensors at the point of entry of the electrodes into the gel, the strip electrode, the grid and depth electrodes. We also used preliminary results of numerical simulations to inform our choice of temperature recording sites [38]. In light of these results the temperature sensors were sited at the following positions for experiment set A (Figure 2): the tip of the most distal (#1) and middle (#4) contacts of the 8-contact depth electrode on the LHS, the corner of the grid (contact #48) and at a reference position within the neck region of the phantom away from all electrodes. For experiment sets B-C (Figure 3): the distal contact (#1) of the 8-contact depth electrode on the LHS the distal contact (#1) of the 6-contact depth electrode on the RHS and two of the corner contacts of the electrode grid (contact s 1#, #41). The temperature-sensor fibre tips were of comparable scale to the electrodes [17], ensuring they were sensitive to localised temperature changes adjacent to the electrode. The sensors were placed such that they lay in a transverse position relative to the electrode contacts to minimise measurement error [17,39].

Temperatures at each measurement point were recorded at a rate of 0.5Hz from one minute prior to MR scanning (baseline period) to 4 minutes after the end of scanning and the maximum temperature increases relative to mean baseline within this period determined.

Scanning protocols - 3 T Siemens TIM Trio

Experiments A-C were performed using a Siemens 3 T TIM Trio MRI system (software level VB13 SP2) (Siemens AG, Erlangen, Germany), firstly, using a transmit/receive birdcage head coil (USA instruments, Aurora, Ohio), and secondly, using the manufacturer-supplied body-transmit coil together with the posterior half of a 12-element head-receive coil for signal reception. The TQ-engine gradients provide maximum gradient amplitudes of 40 mT/m (x and y gradients) and 45 mT/m (z gradient), with a minimum 200μs rise time to full strength. For EPI, gradient amplitudes were typically 25mT/m with rise times of 160μs. Two MRI pulse sequences were applied: Firstly a high-SAR, fast spin-echo (FSE) imaging sequence with a scan duration of 6 minutes and the following parameters: TR 6000ms; TE 106ms; Bandwidth (BW) 81.9kHz; FOV 20 x 20cm; 20% PE oversampling; matrix 512 x 410; 13-18 slices; slice thickness (ST) 3mm; slice spacing (SS) 0.3mm; number of excitations (NEX), or averages 2, echo-train length (ETL), or turbo factor, 17. The scanner-predicted SAR values were 2.4±0.1W/Kg head-average and 1.2W/Kg exposed volume-average for the head and body transmit coils respectively. Secondly a gradient-echo EPI sequence was applied with parameters TR 2900ms; TE 30ms; echo spacing 500μs; 192mm FOV; matrix 64 x 64; 48 slices; ST 2mm; SS 1mm. This gave scanner-predicted SARs of 0.6W/Kg head-average for the head coil and 0.3W/Kg exposed average for the body coil. Experiment set A described above was tested with both head- and body-transmit coils, sets B-C with only the head transmit RF coil.

Scanning protocols - General Electric 3 T Excite

Experiment A was additionally performed using a GE 3 T Excite system (software level 12_M4) using the standard transmit/receive birdcage head coil only, and in this case a head gradient coil set (maximum gradient strength 50mT/m; slew rate 150T/m/s). A 6-minute FSE acquisition with a SAR of 2.5W/Kg (scanner-predicted

head-coil average) was performed. Sequence parameters were: TR 6000; TE 102; BW 31.5kHz; FOV 22 x 22; matrix 512 x 256; 17 slices; ST 5 mm; SS 1.5 mm; averages 2. A gradient-echo EPI sequence was also performed with: TR 3000ms; TE 30ms; echo spacing 580μs; 240mm FOV; matrix 64 x 64; 43 slices; ST 3.0mm; SS 0mm. This gave a scanner-reported SAR of 0.6W/Kg head-average.

Scanning protocols – 1.5 T Siemens TIM Avanto

Experiments A-C were again performed using a Siemens 1.5 T TIM Avanto MRI system (software level VB15 SP2) (Siemens AG, Erlangen, Germany), using a transmit/receive birdcage head coil (USA instruments, Aurora, Ohio).

The TQ-engine gradients are specified as above for the Siemens 3 T TIM Trio. Two MRI sequences were used: 1) A high-SAR, FSE sequence with a duration of 6 minutes 18s, with the following parameters: TR 3700ms; TE 106ms; Bandwidth (BW) 82.6kHz; FOV 20 x 20cm; 20% PE oversampling; matrix 512 x 410; 17 slices; slice thickness (ST) 3mm; slice spacing (SS) 0.3mm; NEX 2, ETL 17. The scanner-reported SAR values were 2.4±0.1W/Kg head-average. 2) A gradient-echo EPI sequence typical of fMRI acquisitions at 1.5 T with the following parameters: TR 4000ms; TE 50ms; echo spacing 690μs; 192mm FOV; matrix 64 x 64; 43 slices; ST 2.0mm; SS 1mm. This yielded a scanner-reported SAR of 0.1W/Kg head-average.

Voltage measurements

Voltage measurements were performed within the 3 T Siemens Tim Trio scanner only. The EPI and FSE sequences described were played-out and voltage measurements performed with the icEEG cables connected and positioned so that they ran proximal to the test-object body as in Figure 2b. Voltages were measured using a balanced coaxial probe [18,40] consisting of two 20:1 ‘low impedance’ probes (950Ω resistors in series with 50 Ω coaxial cables), with shields from each probe periodically joined to minimise ground loops, connected to a 200 MHz digital

oscilloscope (Tektronix TDS 2022, Tektronix Inc., Beaverton, OR, USA) configured with differential inputs. The voltages between the cable termination connected to the most distal LHS 8 contact depth electrode and the cable termination connected to the most distal RHS 6 contact depth electrodes were measured. Then the voltage was measured between the cable terminations connected to the distal corner grid electrodes (contacts #1 and #41) with the circuit completed at the amplifier. These measurements aimed to maximise the loop area (i.e. represent the worst-case condition). Lastly, in order to assess the contribution of signals induced in the test leads to the total voltages detected, a control measurement was performed in which the ends of the balanced probes were connected directly to each other (i.e. probe short-circuited) but left in the same position during scanning as for all previous measurements.

Forces on the implant

The 3 T Siemens Tim Trio scanner was run using both of the sequences described above both while the electrodes were observed visually and while holding the electrodes. Images were reviewed for any movement-related artefact.

Results

Temperature measurements

In all cases with more than one temperature sensor on an electrode, only the values from the contact where the greatest temperature change (∆T) was measured are reported. The maximum observed ∆Ts are summarised in Tables 1-4, and discussed in detail below. Maximum ∆T curves, obtained in this case with the amplifier connected, are shown in Figure 4.

Siemens 3 T TIM Trio - Head transmit coil

The maximum ∆Ts obtained for the FSE sequence with cables attached and placed in different positions within the scanner bore (experiment set A) are summarised in Table 1. Only small ∆Ts were observed using the head-transmit coil, with the maximum ∆T (+0.6ºC) obtained when the cables were arranged to run back past the body (Figure 2b) and terminated in conductive paste to create a short circuit. Temperature increases were lower with the cables lying along the z-axis (+0.4ºC), and in the open circuit configuration the maximum ∆T was similar (+0.3ºC), i.e. within the precision of the temperature measurement (±0.1ºC).

The variation in ∆T due to changing the terminating impedance at the amplifier end of the cables (experiment set B, Figure 3) is shown in Table 2. For the 3 different terminations (amplifier, short- and open-circuit) ∆T was similar. With 180cm cables ∆T was reduced compared to the shorter cable lengths (+0.6ºC) independent of the terminating load. Over the tested range of cable lengths (experiment set C) with the amplifier connected, moderate ∆Ts (≤0.9ºC) were obtained for all cable terminations (Table 3 and Figure 4a). The location and magnitude of greatest heating varied with both cable length and termination. The highest ∆T (+0.9ºC) was found with the shortest cable length of 80cm, the lowest (+0.4ºC) was found with the 150cm cable length.

A 10-minute gradient echo EPI scan was obtained for each cable length connected to the EEG amplifier. Temperature changes (≤0.2ºC) were detected (Table 4, Figure 4a) although their magnitude was of a similar order to baseline temperature fluctuations (in experiment set A, at a control location away from the implants).

Siemens 3 T TIM Trio system - Body transmit coil

The maximum ΔTs obtained within the Siemens TIM Trio using the body-transmit RF coil with cables attached and arranged in different positions within the scanner bore (experiment set A) are again summarised in Table 1. The body RF coil produced larger ΔTs than the head transmit coil. The greatest ΔT (+6.9ºC) was obtained with the FSE sequence and the cables lying 'along Z' as in Figure 2a. The ΔT was smaller (+3.7ºC) for this arrangement with the cables terminated in an open circuit. By rearranging the cables to run back past the body (Figure 2b) ΔT was further reduced (+1.5ºC short-circuit, +0.6ºC open circuit). However, on deliberate placement of the cables in close proximity to the body coil ΔT increased (+2.9ºC).

For the 10-minute EPI scan with a lower SAR (see Table 4), significant heating was observed with the cables attached (+1.8ºC), though the greatest ΔT was smaller compared to the higher-SAR FSE sequence.

GE 3 T Signa Excite system - Head transmit coil

The maximum ΔTs obtained from the phantom using the GE 3 T system with cables attached and placed in different positions within the scanner bore (experiment set A) are also summarised in Table 1. The maximum ΔT with the FSE sequence was +0.9ºC with the cables along the z-axis and was similar (+0.8ºC) when the cables were run past the body and terminated in a short-circuit. For the 10-minute EPI scan (Table 4) no significant ΔT (≤0.1 ºC) was observed.

Siemens 1.5 T TIM Avanto - Head transmit coil

The maximum ΔTs obtained with the Siemens TIM Avanto with cables attached and placed in different positions within the scanner bore (experiment set A) are summarised in Table 1. They follow the same pattern as the results from the 3 T Siemens system (differing by ≤0.2ºC over the tested configurations). FSE-sequence ΔTs were limited to +0.5ºC when the cables lay along Z (as in Figure 2a) in the short circuit configuration, with a reduction to +0.3ºC with an open circuit. Heating was increased when the cables were run past the body (as in Figure 2b) and a temperature change of +2.7ºC was achieved by placing the cables under the head along the coil floor.

The temperature variation due to changing the cable terminating load (experiment set B) is shown in Table 2. A moderate temperature increase (+1.0±0.1ºC) was found over all terminating loads with a 100cm cable length. For the 180cm cable length greater heating (+2.0ºC) was obtained for the short circuit condition than for the open circuit (+1.6ºC) or with the amplifier connected (+1.7ºC). Over the tested range of cable lengths (experiment set C), shown in Table 3, moderate ΔTs of ≤2.0ºC were obtained for all cable lengths. The location and magnitude of greatest ΔT varied with both cable length and termination as at 3 T. A smaller ΔT of +0.9ºC was found with the amplifier connected at the shortest cable length of 80cm, increasing to +1.7ºC at 150cm cable length (Figure 4b).

At 1.5 T a 10-minute EPI scan was obtained at each cable length with the amplifier plugged in. Temperature changes (+0.1ºC) were at the level of measurement precision due to the much lower SAR (0.1W/Kg head-average) of this pulse sequence at 1.5 T (Table 4, Figure 4b).

Voltage measurements

Representative voltage time-courses are shown in Figure 5 and a summary of the maximum peak-to-peak and rms values is given in Table 5. For the circuit comprising the depth electrodes, cables and phantom the peak gradient-switching induced

voltage was 0.04V. Similarly for the grid electrode circuit the peak gradient induced voltage was 0.03V. In the control condition, where the voltages measured originated in the measurement circuit alone a peak voltage of 0.01V was observed, while the peak gradient induced voltage was 0.01V.

Forces on the implant

Visual and tactile monitoring of the electrodes during image acquisition did not reveal any vibration or flexion of the electrodes. No vibration- or displacement-related artefact was observed on the images.

Discussion

The potential hazards involved in performing fMRI while recording from icEEG electrodes were examined in order to determine whether, and under which circumstances, this did not introduce a significant additional health risk. Induced currents due to movement through the static B_0 field are theoretically small and the associated potential risk low. No electrode flexion due to transient magnetic effects was observed. We identified a theoretical risk of neuronal depolarisation due to gradient-switching induced currents, and of tissue heating due to interaction with the RF fields used for imaging. These 2 principle hazards were therefore examined experimentally by *in vitro* measurements of voltage and temperature as will now be discussed.

Tissue heating

Our findings confirmed that under certain circumstances significant tissue temperature rises, substantially exceeding guideline limits, may occur during simultaneous icEEG-MRI, as is the case when imaging these implants solely for electrode localisation [17]. However, our results also show that it is possible to keep tissue-heating within safe limits by the following measures: 1) Using a head transmit coil; 2) careful control of cable position within the coil / scanner bore; 3) using low head-average SAR sequences such as gradient-echo EPI. While the temperature rise at a specific location was found to be highly dependant on field strength, cable termination and electrode properties, certain lengths of electrode and cable were associated with moderately reduced heating over all measured locations and this length was field strength-dependent.

Effect of using a body RF coil

For the body-coil test using the Siemens 3 T TIM Trio, with the cables in the ‘along Z’ position, there was much greater heating (+6.9ºC) than for the other lead positions which can be explained by increased exposure to high RF E-fields proximal to the end of the coil. Significant heating was observed (+2.9ºC) with the cables going past

the body towards the feet and the cables being placed close to the bore. Scaling the maximum ΔT produced relative to the SAR limit gives a much larger peak ΔT for the body coil (+18.4ºC, SAR-exposed volume = 3.2W/Kg) compared to the head coil (+2.2ºC, SAR-exposed volume 3.2W/Kg) because although greater power is required for the body coil to produce the same B1 field it is averaged over a greater mass. These results suggest that use of the body coil presents a greater risk, in line with our previous observations for MRI for intracranial electrode localisation [17]. Also, since movement of the patient bed during a scanning session alters the implant/patient position relative to the body transmit-coil (which has a fixed z-position) safety tests would be required over the possible range of patient locations along this axis. Therefore no further tests were performed using the body-transmit RF coil.

Effect of cables and their properties on tissue heating

In contrast to our previous study involving MRI of isolated icEEG electrodes [17], the effect of introducing the EEG recording equipment and connecting cables was examined. Three different factors were hypothesised to influence heating: A) cable position within the scanner bore, B) cable termination properties and C) cable length.

In relation to cable position, for the head-transmit RF coil highly consistent results were obtained across the 3 scanner platforms. We found that with 120cm length cables heating remained moderate (<1.0ºC) with the FSE sequence used provided that the cables exited the RF coil along its central z-axis. In general, heating was also moderate when the cables were run back past the body (<1.0ºC). However, heating was increased by deliberately placing the cables in close proximity to the head RF coil. Since positioning the cables close to the body increases the chances of accidental placement close to the RF coil and also increases variability due to differences in patient geometry, this practice is should be avoided. Placement of the cables along the z-axis of the scanner reduces these risks. The results from the 1.5 T and 3 T Siemens scanners were highly consistent (within 0.2ºC), and similar values

were obtained on a 3 T GE scanner suggesting that the advantages of routing the cable along the central z-axis of the head coil (corresponding to the theoretical minimum of the E-field for an unloaded birdcage coil) are applicable across scanners with similar head transmit coils.

On varying the cable termination, differences in maximum heating over all cable lengths investigated were relatively small (a factor of 2 - see Table 2) and the maximum heating was in all cases moderate (+1.1ºC at 3 T and +2.0ºC at 1.5 T). However, the particular implant/location where maximum temperature changes occured did change (as previously found for electrodes not attached to cables).

The effect of cable length varied with field strength (Table 3). At 1.5 T the maximum heating for any given configuration was found to be lowest for the shorter cable lengths (80-100cm) with a total wire length outside the phantom in the range 145-185cm. In contrast, at 3 T the maximum heating was lower for longer cables (150cm). This may be ascribed to the relationship between cable length and resonant heating found for individual wires [30]. However, the tested implants are relatively complicated structures with multiple internal wires of varying lengths and different shape and size electrode contacts, making it difficult to make general statements about safe lengths. Instead we have tested a number of different implants (with associated differences in implant length, depth of insertion and location) and cable properties (length and termination) aiming to sample sufficient combinations of these factors to make it unlikely that an untested combination will result in heating above the levels found here. We found that maximum heating over all locations was moderate and varied by a factor of 2 over the range of tested cable lengths and terminations tested, while heating from individual locations was more variable. Hence while it may be possible to choose cable lengths to minimise heating, it is prudent to specify safety limits which account for heating over the full range of conditions (electrode types, termination, cable length) to avoid the possibility of injurious heating due to unforeseen differences between tested and actual conditions. For patient

studies it remains possible that a greater range of implant location and depth of insertion could be encountered hence we recommend a safety margin similar to that used for imaging unconnected implants for localisation purposes [17]. For implant arrangements that substantially deviate from conditions tested here additional safety testing may be required before imaging can proceed.

Effect of cables compared to isolated electrodes on tissue heating

We found connecting the electrodes to an amplifier produced similar levels of implant heating to the situation without cables [17] and varied with cable length. This result is consistent with safety measurements involving external cardiac pacemaker pulse generators where connection of pacing leads to the pulse generator resulted in decreased heating [41]. Hence, the addition of the amplifier circuitry does not necessarily result in an increased risk of intracranial electrode heating.

Comparison of EPI and FSE results

The ratio of the heating produced by the FSE to that due to the EPI sequence was, as expected, close to the ratio of the head/exposed volume SAR for each sequence (Table 4). Provided the head coil was used, the fMRI EPI protocol produced a very low temperature increase well within the guidelines.

Experimental considerations

Our measurements broadly follow the principles of ASTM F 2182-02a [34], a standard for testing MRI-induced temperature increases near passive elongated implants [41]. However, the field distributions within our phantom may not accurately represent the exact field distribution found within a human body. Simulation studies (e.g. see reference [48]) may help to quantify these differences. This, combined with the RF coil specific patterns which themselves are radically altered by the introduction of implants makes the determination of absolute ‘worst case’ or ‘typical’ implant positioning difficult [33, 42]. In previous work, we showed that temperature changes were highly reproducible given a fixed electrode lead configuration, the main

source of uncertainty being due to differences in electrode position within the phantom [17]. This was addressed in this study by using a large number of electrodes, thereby covering a larger range of implantation configurations and increasing the likelihood that the worst case position is tested. Other sources of potential error in the temperature measurements include the limited MRI sequence duration. A 6-minute structural sequence was chosen because it corresponded to the duration of the IEC SAR limit [43] which was developed based on the time required for thermal equilibrium to be achieved in the body. EPI scans were 10 minutes and this is the likely uninterrupted duration that would be desirable for icEEG-fMRI acquisitions.

Using a similar setup as the one used in this work, a 500% uncertainty in temperature values was reported, linked to non-optimal positioning of the temperature-sensing optical-fibre tips relative to the electrode contacts [39]. In our study the temperature probes were therefore positioned transversely relative to the electrode contacts enabling reproducible measurements [17,39]. Uncertainty in the physical properties of the phantom gel may have added to uncertainty in temperature measurements, although this effect is likely small considering the consistency of results obtained in this and our previous study [17]. Furthermore, deviation from central placement of the head in the head coil or alternative patient positions in the head coil could cause significantly different heating.

As already noted the cable and electrode lead arrangement within the transmit coil is a significant factor in determining ΔT leading to the recommendation of a tightly controlled experimental protocol with fixed lead and cable geometry conforming to previously tested configurations. In particular, specific additional tests would be required to address the safety of MRI when not all of the electrodes are connected although significantly increased heating above that found when either all are connected or all unconnected would seem unlikely. While we believe the observed ΔTs observed here to be accurate we cannot totally exclude the possibility that

greater heating occurred at electrode positions we were unable to monitor. However, our experiments were designed to minimise this risk. Our observations of tissue heating may be considered conservative, i.e. over-estimates compared with the likely *in vivo* situation for number of reasons: firstly, the gel phantom used is a conservative model for tissue heating; it is expected that ΔTs would be smaller *in vivo* since brain temperature is regulated by perfusion [44,45]; a large number of electrodes were tested simultaneously to increase the possibility of resonant loop and/or antenna formation; the electrode tail / cable terminations were shorted to test a 'fault condition' where conductive loops are formed; a pulse sequence was chosen to provide a head-average SAR close to the statutory limits. The reduction in heating due to perfusion depends on the rate of local heating relative to the rate of heat dissipation. Hence the steady state heating realized *in vivo* can be estimated from gel phantom studies like ours as the heating found at a time from the sequence start equal to the tissue time-constant, which for brain is estimated in the range 72-150s [46]. Reading from figure 4 this would suggest a reduction in heating of approximately 20% for an electrode within perfused brain tissue.

Using gradient-echo EPI at 3 T with a SAR of 0.6W/Kg resulted in a maximum temperature increase of 0.3ºC+/-0.1ºC demonstrating that provided the specific experimental arrangement is replicated *in vivo* (head coil, the same scanner, pulse sequence, head average SAR, cable arrangement etc) the additional health risk associated with RF heating is very small. At 1.5 T the SAR of a standard fMRI protocol was 0.1W/Kg and temperature was below our experimental thermometry precision (≤0.1ºC). We note that to cause irreversible tissue damage it would be necessary to maintain substantially greater heating (to 42ºC) for roughly one hour [47]. Thus for highly perfused brain tissue damaging levels of heating must be considered extremely unlikely.

Generalisation of findings

Our results demonstrate that the position of the cables for maximum safety varied little between 1.5 T and 3 T but heating was highly sensitive to their position relative to the RF coil. Variability in maximum heating over all locations due to cable length and termination was a factor of 2 (sets B-C) on both scanners although heating was lower for the 3 T Tim trio system. This may be due to the scanner-dependent SAR estimation methods leading to different heating for nominally identical experimental arrangements [48, 49]. Therefore, SAR limits for safe MRI operation in the presence of intracranial electrodes cannot be generalised across MRI scanners without careful cross-scanner calibration [48, 49]. In particular we note that even if calorimetric measurements were performed to cross-calibrate scanner-reported average SAR between systems, hardware-dependent variations in interactions between the MRI RF field and conducting implants might still lead to significant variations in the resulting tissue temperature increases. It is therefore more useful to consider a SAR limit based on the expected temperature changes for a specific range of implantation configurations, RF coil, scanner, implant and cabling arrangement. This is different to the approach that might be considered for general safety guidelines for the purposes of device labelling [41,33]. Hence, a local safety assessment and strict adherence to a fixed experimental protocol is important if MRI is to be performed without significant additional risk in patients while recording from intracranial EEG electrodes. Finally, we note that neither the electrodes (Ad-Tech medical) used here, nor the EEG equipment (Brain Products) has been designed for the purpose of recording intracranial EEG during MRI and they do not have FDA, European Union or similar certification for this purpose.

Tissue stimulation

Our main finding was that the measured voltage at frequencies that could cause tissue stimulation was small (0.04±0.01V). Voltage measurements were made across

two different circuits comprising of the implant and the tissue primarily aimed at determining the likely voltages induced in these circuits due to gradient switching. During normal operation, the EEG amplifier's input impedance (typically >1MΩ) limits the amount of current flowing through the subject at low frequencies; for example, for the maximum induced electromotance observed in this study, 0.04V, the current should be <0.04μA. However, in a fault condition, the majority of the impedance would be provided by the tissue and in this case larger currents could result. For both tested circuits the voltage was 0.04±0.01V. Assuming a conservatively low tissue impedance value of 500Ω, this corresponds to a current of 0.08mA, well below the medical devices limit for a single-fault condition (0.5mA) and far less than the initial stimulation voltage stipulated to provoke a seizure of 2V ([50]; see appendix A). The induced surface charge density derived from the voltage measurement is some 400 hundred times smaller than the estimated worse case. Using the measured voltage and parameter values described in the theory section (gradient switching time of 200μs, electrode area 0.07cm^2, tissue impedance 500Ω) we get an estimated surface charge density of 0.2μC/cm^2. This is consistent with results obtained for a DBS electrode with an external pulse generator sited outside the scanner room with long connecting leads attached [21]. The worst-case theoretical estimate is therefore considerably larger than the experimental values obtained here because the exposed loop area is moderately less than the possible maximum used for calculation and it lies approximately in the centre of the gradients where the dB/dt is much smaller; the estimate assumed a position 1m from isocentre, at the edges of the useful gradient fields. If patients were deliberately or accidentally placed away from the magnet isocentre, or if an arrangement of leads introduced the possibility for greater loop area, greater induced voltages might result requiring more stringent safety precautions. We did not consider conductive loops resulting from the connection of both the patient and EEG amplifier to true ground since compliance of the EEG equipment with guidelines [29] requires all patient applied parts to be electrically

isolated from true ground. Furthermore, the amplitude of gradient switching for the routine fMRI sequence is considerably lower than the absolute limits of the scanner with all three gradient direction switched simultaneously (used for the estimation). However the sequence we used was close to the limits of gradient-switching rate imposed to prevent peripheral nerve stimulation (PNS) and so dramatically greater rates of gradient switching are not possible. These combined factors account for the difference between the theoretical worse case and the measured gradient induced voltage. Magnetic field gradient performance was very similar on the 1.5 T and 3 T Siemens scanners and this taken together with field strength independent PNS limits suggests that these results should be consistent across field strengths.

In summary, in relation to stimulation we have shown that in the worst case theoretical risk due to magnetic gradient field switching when there is a short circuit due to an amplifier or lead fault; however, the actual measured gradient-switching induced voltages are not large enough to cause damage or stimulation even in this case.

Conclusions

The greatest potential hazard in performing simultaneous intracranial EEG and fMRI in human patients was found to be RF-induced tissue heating in the proximity of the depth and grid electrode contacts. In certain circumstances, heating well above guideline limits was observed. However, heating was limited by using a head coil, adding connecting cables, controlling their length and position in addition to running lower SAR sequences. Therefore, we conclude that provided implant and scanner specific SAR limits are observed and that a head RF transmit coil is used, the risk of tissue damage due to electrode-associated RF-induced heating is low. Furthermore, we have shown that magnetic field gradient-induced currents are well below the threshold for tissue stimulation and so tissue damage (requiring a much larger current) will not occur. Hence icEEG-fMRI can be performed without significant additional risk in certain specific circumstances.

As a final caveat it should be noted that we have shown that alternative circumstances exist in which these studies can pose a significant risk of injury to the subjects. Therefore site-specific testing and a conservative approach to safety is required to avoid the risk of adverse events.

Appendix A Safety guidelines - currents

Recommended safe limits for currents in the 1-1000Hz range, within MRI gradient switching frequencies, are a maximum of 0.1mA under normal conditions and 0.5mA under single fault conditions [29]. This can be placed in the context of the recommended charge density limit for chronic therapeutic neuronal stimulation [28,50-51] of 30 $\mu C/cm^2$ (where non-continuous this is the average over a pulse width) and cortical stimulation studies for seizure provocation: the recommended initial stimulation parameters are 2V, 0.5mA, 152ms pulse duration, 40 per second, 5 seconds [52]. These parameters exceed guidelines, which deliberately lie below the level required for stimulation. It should be noted that tissue-heating also results from current flow at these frequencies but the threshold for depolarisation related effects lie well below those for significant thermal effects [27].

At RF frequencies pertinent to MRI B1-fields, the relevant medical-device current limit is 10mA root mean squared (rms) [29] although this is a default value for frequencies >100KHz and so its direct relevance in the RF frequency range of MRI systems (128Mhz at 3Tesla) is questionable [27]. Indeed this value can be contrasted with the higher contact current limits (20-45mA) derived for public exposure to RF frequency fields [53,54]. It must be remembered that current *per se* does not fully reflect the likelihood of injury because the electrode contact area and shape determining the current density are critical factors. RF burns have been observed when the current density exceeds $250mA/cm^2$ [55]. From diathermy it is known that the nature of damage caused is related to the temporal characteristics of the current in addition to its spatial distribution. Continuous currents are more likely to cause cutting and vaporisation while pulsed currents cause coagulation because the latter (like those induced by MRI RF pulses) cause more distributed heating [25-26].

Appendix B Safety guidelines - temperature increases

Excessive tissue temperature increases are hazardous as they can cause cell damage and ultimately cell death. The rate at which this process occurs is governed by the absolute temperature and the duration of exposure, rate of heating and the cell type [47]. Relatively little data exists on the long term effects of small temperature elevations (39-42ºC) in the brain, however at the upper end of this range most cells require long exposure times (many hours) to die [47]. The IEC limits state that brain temperature should not exceed 38ºC [43] implying an allowable increase of <1ºC and providing a conservative limit substantially below the temperature elevation required for neuronal cell damage over typical scan durations (0.5-1.5 hours). The relationship between Joule heating expressed in terms of SAR (W/kg) and the RF electric field is given by:

$$SAR = \frac{\sigma}{2\rho}\left|\vec{E}\right|^2 \qquad [5]$$

Where σ is the conductivity of the medium (S/m), ρ is the mass density (kg/m3). The SAR can in turn be related to temperature changes (∆T) in a given medium by considering the rate of heating in the absence of thermal losses where C_p is the specific heat capacity.

$$SAR = C_p \frac{dT}{dt} \qquad [6]$$

MRI-related safety guidelines specify SAR limits intended to restrict tissue temperature increases to within the levels described above, but these are specifically formulated for implant-free subjects. Historically to maintain MRI safety, SAR limits were specified making conservative assumptions about thermoregulation, rather than using absolute tissue temperature limits due to the practical difficulties of accurate determination or prediction of local tissue temperature *in vivo* [56]. The current head-average SAR limits are 3.2W/Kg for a 6-minute exposure period [43] or 3W/Kg for a 5-minute exposure period [39]. For short periods guidelines [43] allow three times this value averaged over any 10s although clinical scanners generally do not permit

scans to be prescribed with greater SAR than the limits for 5-6minute exposure periods. For implants shorter duration / higher SAR limits are potentially more dangerous because most of the heating will occur within the first minute of exposure. The local SAR should not exceed 10W/Kg averaged over 10g of tissue (IEC) [43] or 8W/Kg over 1g of tissue (FDA) [57]. One gram of tissue will typically correspond to a volume of the order of ~1cm^3 in the human brain, which is relatively large compared to many implants and in particular those studied here; no safety limit exists for smaller masses or volumes. Temperature is simple to measure in test objects and is the direct variable corresponding to potential tissue injury from exposure to RF fields at the spatial scale of the electrode contacts [27]. The above considerations lead us to measure temperature increases over small volumes (~1mm^3) proximal to the implant as the best determinant of risk and for the subsequent prescription of a procedure that is likely to stay within heating limits.

References

1. Duncan JS. Epilepsy surgery. Clin Med. 2007 Apr;7(2):137-42.
2. Lachaux JP, Rudrauf D, Kahane P.J. Intracranial EEG and human brain mapping. Physiol Paris. 2003 Jul-Nov;97(4-6):613-28.
3. E. Halgren, K. Marinkovic and P. Chauvel, Generators of the late cognitive potentials in auditory and visual oddball tasks. Electroencephalogr. Clin. Neurophysiol. 106 (1998), pp. 156–164.
4. Ives JR, Warach S, Schmitt F, et al. Monitoring the patient's EEG during echo planar MRI. Electroencephalogr Clin Neurophysiol 1993; 87:417–420.
5. Laufs H, Duncan JS. Electroencephalography/functional MRI in human epilepsy: what it currently can and cannot do.Curr Opin Neurol. 2007 Aug;20(4):417-23.
6. Salek-Haddadi A, Diehl B, Hamandi K, Merschhemke M, Liston A, Friston K, Duncan JS, Fish DR, Lemieux L. Hemodynamic correlates of epileptiform discharges: an EEG–fMRI study of 63 patients with focal epilepsy. Brain Res 2006; 1088:148–166.
7. Gotman, J., Kobayashi, E., Bagshaw, A.P., Benar, C.G., Dubeau, F., 2006. Combining EEG and fMRI: a multimodal tool for epilepsy research. J. Magn. Reson. Imaging 23 (6), 906–920.
8. Laufs H, Daunizeau J, Carmichael DW, Kleinschmidt A. Recent advances in recording electrophysiological data simultaneously with magnetic resonance imaging. Neuroimage. 2008 Apr 1;40(2):515-528.
9. Laufs H, Holt JL, Elfont R, Krams M, Paul JS, Krakow K, Kleinschmidt A. Where the BOLD signal goes when alpha EEG leaves. Neuroimage. 2006 Jul 15;31(4):1408-18.
10. Laufs H, Lengler U, Hamandi K, Kleinschmidt A, Krakow K. Linking generalized spike-and-wave discharges and resting state brain activity by

using EEG/fMRI in a patient with absence seizures. Epilepsia. 2006 Feb;47(2):444-8.

11. E. Halgren, K. Marinkovic and P. Chauvel, Generators of the late cognitive potentials in auditory and visual oddball tasks. Electroencephalogr. Clin. Neurophysiol. 106 (1998), pp. 156–164.
12. Logothetis NK, Pauls J, Augath M, Trinath T, Oeltermann A. Neurophysiological investigation of the basis of the fMRI signal. Nature. 2001 Jul 12;412(6843):150-7.
13. Lemieux L, Laufs H, Carmichael D, Paul JS, Walker MC, Duncan JS. Noncanonical spike-related BOLD responses in focal epilepsy. Hum Brain Mapp. 2008 Mar;29(3):329-45.
14. Hawco CS, Bagshaw AP, Lu Y, Dubeau F, Gotman J. BOLD changes occur prior to epileptic spikes seen on scalp EEG. Neuroimage. 2007 May 1;35(4):1450-8.
15. Federico P, Abbott DF, Regula S, Briellmann A, Harvey S, Jackson GD. Functional MRI of the pre-ictal state Brain 2005 128(8):1811-1817;
16. Archer JS, Waites AB, Abbott DF, Federico P, Jackson GD. Event-related fMRI of myoclonic jerks arising from dysplastic cortex. Epilepsia. 2006 Sep;47(9):1487-92.
17. Carmichael DW, Thornton JS, Rodionov R, Thornton R, McEvoy A, Allen PJ, Lemieux L. Safety of localising epilepsy monitoring intracranial EEG electrodes using MRI: Radiofrequency-induced heating. J Magn Reson Imaging. 2008 Oct 28;28(5):1233-1244.
18. Lemieux L, Allen PJ, Franconi F, Symms MR, Fish DR. Recording of EEG during fMRI experiments: patient safety. Magn Reson Med. 1997 Dec; 38(6):943-52.
19. Finelli DA, Rezai AR, Ruggieri P, Tkach J, Nyenhuis JA, Hrdlicka G, Sharan A, Gonzalez-Martinez J, Stypulkowski PH, Shellock FG. MR-related heating

of deep brain stimulation electrodes: An in vitro study of clinical imaging sequences. Am J Neuroradiol, 2002; 23:1795–1802.

20. Rezai AR, Finelli D, Nyenhuis JA, Hrdlicka G, Tkach J, Sharan A, Rugieri P, Stypulkowoski PH, Shellock FG, 2002. Neurostimulation systems for deep brain stimulation: In vitro evaluation of magnetic resonance imaging-related heating at 1.5 T. J Magn Reson Imaging 15:241-250.
21. Georgi JC, Stippich C, Tronnier VM, Heiland S. Active deep brain stimulation during MRI: A feasibility study. Magn Reson Med, 2004; 51:380–388.
22. Rezai AR, Baker KB, Tkach JA, Phillips M, Hrdlicka G, Sharan AD, Nyenhuis J, Ruggieri P, Shellock FG, Henderson J. Is magnetic resonance imaging safe for patients with neurostimulation systems used for deep brain stimulation? Neurosurgery, 2005; Nov;57(5):1056-62.
23. Carmichael DW, Pinto S, Limousin-Dowsey P, Thobois S, Allen PJ, Lemieux L, Hariz M, Yousry T, Thornton JS. Functional MRI with active, fully implanted, deep brain stimulation systems: Safety and experimental confounds. Neuroimage, 2007; Aug 15;37(2):508-17.
24. Baker KB, Nyenhuis JA, Hrdlicka G, Rezai AR, Tkach JA, Shellock FG. Neurostimulation systems: assessment of magnetic field interactions associated with 1.5- and 3-T MR systems. J Magn Reson Imaging, 2005; 21(1):72-7.
25. Aigner N, Fialka C, Fritz A, Wruhs O, Zöch G. Complications in the use of diathermy. Burns. 1997 May;23(3):256-64.
26. Hay DJ, Electrosurgery. Surgery Volume 23, Issue 2, 1 February 2005, 73-75
27. Litvak E, Foster KR, Repacholi MH. Health and safety implications of exposure to electromagnetic fields in the frequency range 300 Hz to 10 MHz. Bioelectromagnetics. 2002 Jan;23(1):68-82.
28. Kuncel, A.M., Grill, W.M., 2004. Selection of stimulus parameters for deep brain stimulation. Neurophysiology 115 (11), 2431–2441 (Nov.).

29. IEC (2005) International Standard, Medical Equipment Part 1: General requirements for basic safety and essential performance. International Electrotechnical Commission 60601-1:2005, Geneva 2005.
30. Yeung CJ, Karmarkar P, McVeigh ER. Minimizing RF heating of conducting wires in MRI. Magn Reson Med. 2007 Nov;58(5):1028-34.
31. Mattei E, Triventi M, Calcagnini G, Censi F, Kainz W, Mendoza G, Bassen HI, Bartolini P. Complexity of MRI induced heating on metallic leads: experimental measurements of 374 configurations. Biomed Eng Online. 2008 Mar 3;7:11.
32. Bhavaraju NC, Nagaraddi V, Chetlapalli SR, Osorio I. Electrical and thermal behavior of non-ferrous noble metal electrodes exposed to MRI fields. Magn Reson Imaging. 2002 May;20(4):351-7.
33. Kainz W. MR heating tests of MR critical implants. J Magn Reson Imaging. Sep;26(3):450-1. 2007.
34. ASTM F 2182-02a. Standard test method for measurement of radio frequency induced heating near passive implants during magnetic resonance imaging. ASTM Committee F04 on Medical and Surgical Materials and Devices, Subcommittee F04.15 on Material Test Methods. West Conshohocken, PA: ASTM International; 2007.
35. Park SM, Nyenhuis JA, Smith CD, Lim EJ, Foster KS, Baker KB, Hrdlicka G, Rezai AR, Ruggieri P, Sharan A, Shellock FG, Stypulkowski PH, Tkach J. Gelled verses Nongelled Phantom material for measurements of MRI-induced temperature increases with bioimplants. IEEE transactions on magnetics, 2003; 39 (5): 3367-3371.
36. Achenbach S, Moshage W, Diem B, Bieberle T, Schibgilla V, Bachmann K: Effects of magnetic resonance imaging on cardiac pacemakers and electrodes. Am Heart J 134:467–473, 1997.

37. Pictet, Meuli R, Wicky S, van der Klink JJ. Radiofrequency heating effects around resonant lengths of wire in MRI. Physics in Medicine and Biology 47(16):2973-85, 2002.
38. Carmichael DW, Hand J, Li Y, McEvoy A, Lemieux L. Estimating Specific Absorption Rate (SAR) during MRI in the human brain with intracranial EEG electrodes used for Epilepsy monitoring: A preliminary study using finite integral technique (FIT) modelling. Proc. International meeting of the ISMRM 2008 (Toronto), 1061.
39. Mattei E, Triventi M, Calcagnini G, Censi F, Kainz W, Bassen HI, Bartolini P. Temperature and SAR measurement errors in the evaluation of metallic linear structures heating during MRI using fluoroptic probes.Phys Med Biol. 2007 Mar 21;52(6):1633-46.
40. Smith DC, 1993 High frequency measurements and noise in electronic circuits. Van Nostrand Reinhold, New York.
41. Shellock FG. Comments on MR heating tests of critical implants. J Magn Reson Imaging. Nov;26(5):1182-5. 2007.
42. Bassen HI, Kainz W, Mendoza G, Kellcom T. MRI-induced heating of selected thin wire metallic implants: laboratory and computational studies - findings and new questions raised. Minim Invasive Ther Allied Technol 2006; 15: 76-84.
43. International Electrotechnical Commission (IEC), Medical electrical equipment – particular requirements for the safety of magnetic resonance equipment for medical diagnosis. IEC 60601-2-33, 1995 revised 2002.
44. Salcman M, Moriyama E, Elsner HJ, Rossman H, Gettleman RA, Neuberth G, Corradino G, Cerebral blood flow and the thermal properties of the brain: a preliminary analysis. J Neurosurg. 1989; Apr;70(4):592-8.
45. Collins CM, Smith MB, Turner R, Model of local temperature changes in brain upon functional activation. J Appl Physiol. 2004; Dec; 97(6):2051-5.

46. Akca IB, Ferhanoglu O, Yeung CJ, Guney S, Tasci TO, Atalar E. Measuring local RF heating in MRI: Simulating perfusion in a perfusionless phantom. J Magn Reson Imaging. 2007 Nov; 26(5): 1228-35.
47. Dewhirst MW, Viglianti BL, Lora-Michiels M, Hanson M, Hoopes PJ. Basic principles of thermal dosimetry and thermal thresholds for tissue damage from hyperthermia, International Journal of Hyperthermia, 2003; 19:3, 267 – 294.
48. Baker KB, Tkach JA, Nyenhuis JA, Phillips M, Shellock FG, Gonzalez-Martinez J, Rezai AR. Evaluation of specific absorption rate as a dosimeter of MRI-related implant heating. J Magn Reson Imaging 20:315–320. 2004.
49. Baker KB, Tkach JA, Phillips MD, Rezai AR.Variability in RF-induced heating of a deep brain stimulation implant across MR systems. J Magn Reson Imaging. Dec;24(6):1236-42. 2006.
50. Agnew WF, McCreery DB. Considerations for safety with chronically implanted nerve electrodes. Epilepsia. 1990;31 Suppl 2:S27-32. Review.
51. McCreery DB, Agnew WF, Yuen TG, Bullara L. Charge density and charge per phase as cofactors in neural injury induced by electrical stimulation. IEEE Trans Biomed Eng. 1990 Oct;37(10):996-1001.
52. Niedermeyer E. Ch. 8 Depth Electroencephalography, in Epilepsy: A comprehensive textbook. Ed. Engel J. and Pedley TA, Lippincott-Raven, Philadelphia, 1997.
53. ICNRP. Guidelines for limiting exposure to time varying electric, magnetic and electromagnetic fields (to 300GHz), 1998.
54. IEEE C95.1-1999 IEEE Standard Safety Levels with Respect to Human Exposure to Radio Frequency Electromagnetic Fields, 3 KHz to 300 GHz.
55. Brown BH, Johnson SG, Betts RP, Henry L. Burns thresholds to radiofrequency leakage currents from surgical diathermy equipment. J. Med. Eng Technol. 1977; 1, 277-281.

56. ICNIRP (2004). Medical magnetic resonance (MR) procedures: protection of patients. Health Physics, 87(2), 197-216.
57. Shellock FG. Reference Manual for Magnetic Resonance Safety, Implants, and Devices: 2007 Edition. Los Angeles, Biomedical Reference Publishing Group. 2007. p504.

Figure captions

Figure 1 Photographs of the experimental arrangement.

(a): Photographs of the head part of the phantom shown with the various implants inserted adjacent to the full phantom with a 30 cm ruler for scale. The simulated patient right hand side (RHS) and left hand side (LHS) are indicated. The black plastic components were used to position and hold the electrodes. Electrodes indicated with a dashed line (strip and lower LHS depth electrode) were removed for parts experimental parts B-C where the amplifier was used.

Figure 2 Schematic of the experimental arrangement for experiment set A and voltage measurements.

Schematic of the phantom showing the sites of temperature measurement (in red) and the different cable arrangements within the scanner bore: (a) with the cables lying along Z, and (b) with the cables running back passed the body. Two different cable terminations were used for each both open and short circuit. The voltage measurement set up consisting of a 20:1 coaxial probe connected to an oscilloscope outside the scan room is also shown though these measurements were not obtained simultaneously with experiment set A. Measurements of voltage were obtained across the distal contacts of the left and right hand side depth electrodes and across the distal corner grid electrode contacts. N.B. Not drawn to scale.

Figure 3 Schematic of the experimental arrangement for experiment set B-C.

Schematic of the phantom showing the arrangement used for testing the cable termination and cable length. The strip and second depth electrode were removed as compared to the arrangement in Figure 2 and the temperature sensors were place sites of temperature measurement (in red). Three different cable terminations were used; firstly the amplifier was connected as shown, then the amplifier was disconnected from the ribbon cables and removed (open circuit) and lastly one ribbon cable was connected back into the 64x in put box to connect channels 1-32 to 33-64 (short circuit). N.B. Not drawn to scale.

Figure 4 Temperature change graphs showing maximum heating with the amplifier attached and the cables 'along Z' for FSE and EPI pulse sequences

In all sub figures the solid diamonds indicates the FSE sequence (2.4W/Kg) and the crosses the EPI sequence (0.6W/Kg at 3 T and 0.1W/Kg at 1.5 T).

a) Siemens 3 T, head coil, 80cm cables producing the maximum heating when connected to the amplifier, b) Siemens 1.5 T, head coil, 150cm cables producing the maximum heating when connected to the amplifier.

Figure 5 Voltage measurements

The voltage measured during an EPI acquisition between the cable terminations from the left hand side and right hand side depth electrodes most distal (closest) contacts. Note that the scaling has been used to visualise the gradient induced voltage and so the RF induced voltage is clipped. Various features can be seen; the fat saturation pulse (1), the excitation pulse (2) and the readout gradient switching (3).

Scanner	Cable position	Cable termination	Coil (SAR head / body)	ΔT ºC depth	ΔT ºC grid
3T Siemens Trio	Along Z	short circuit	Head (2.4 / 0.2 W/Kg)	0.3	0.4
	Past body	open circuit		0.2	0.3
		short circuit		0.3	0.6
		open circuit		0.2	0.3
	Along Z	short circuit	Body (1.2 / 0.5 W/Kg)	6.9	2.9
		open circuit		3.7	2.2
	Past body	short circuit		0.3	1.5
		open circuit		0.6	0.3
	Past body - along body coil	short circuit		2.9	1.3
1.5T Siemens Avanto	Along Z	short circuit	Head (2.4 / 0.2 W/Kg)	0.4	0.5
		open circuit		0.3	0.2
	Past body	short circuit		0.4	0.8
	Under head - along head coil	open circuit		1.0	2.7
3T GE Signa	Past body	short circuit	Head (2.5 / 0.3 W/Kg)	0.8	0.5
	Along Z	short circuit		0.7	0.9
		open circuit		0.7	0.2

Table 1 Maximum ΔTs with cable position for 3 different MRI scanners. Ambient reference point ΔTs were ≤0.2ºC for all experiments, the measurements precision is ±0.1ºC.

∆T max °C	3T Siemens Trio		1.5T Siemens Avanto	
cable length (cm)	80-180	180	80-180	100
amplifier	0.9	0.6	1.7	1.1
short	1.1	0.6	1.6	1.0
open	1.0	0.6	2.0	1.1

Table 2 Maximum temperature changes (∆T) over all measured locations with different cable terminations. All experiments were conducted with the head coil and a 6 minute 2.4W/Kg imaging sequence.

∆T range °C	Cable length (cm)				
Field strength	80	100	120	150	180
3T	0.3-0.9	0.1-0.7	0.2-0.7	0.2-0.4	0.2-0.6
1.5T	0.3-0.9	0.3-1.1	0.4-1.3	0.4-1.7	0.4-1.1

Table 3 Temperature changes (∆T) at different cable lengths with the amplifier connected. The range of temperature increases over the 4 measured spatial locations is given. All experiments were conducted with the head coil and a 6 minute 2.4W/Kg imaging sequence.

Scanner	Coil	Cables	Termination	Seq / SAR	∆T ºC max
Siemens Trio	Head	80-180cm	Amplifier	EPI / 0.6 / 0.1	≤0.2
				FSE / 2.4 / 0.1	≤0.9
	Body	120cm	short	EPI / 0.3 / 0.1	1.8
				TSE / 1.2 / 0.5	6.9
GE Signa	Head	120cm	open	EPI / 0.6 / 0.2	≤0.1
				FSE / 2.4 / 0.1	0.7
		120cm	short	EPI / 0.6 / 0.2	≤0.1
				FSE / 2.4 / 0.1	0.9
Siemens Avanto	Head	80-180cm	Amplifier	EPI / 0.1 / 0.1	≤0.1
				FSE / 2.4 / 0.1	≤1.7

Table 4 Comparison of maximum ∆T from FSE and EPI imaging sequences over a range of experimental conditions.

Measurement position	peak-peak voltage (V) during EPI gradients
depth	0.04
grid	0.03
control	0.01

Table 5 Summary of peak voltage measurements during gradient switching across left and right hand side depth electrode tips, the distal grid corners, and within the measurement circuit (control).

Figure 1

Click here to download high resolution image

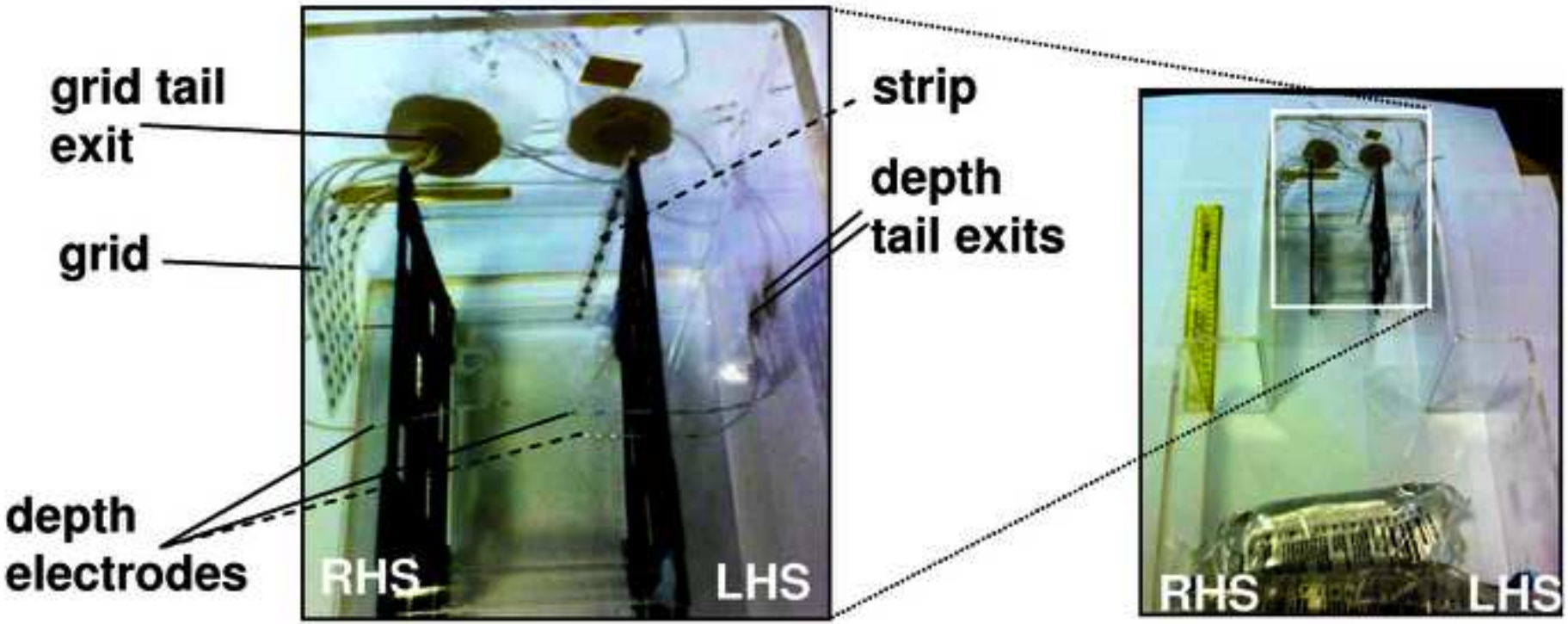

Figure 2

Click here to download high resolution image

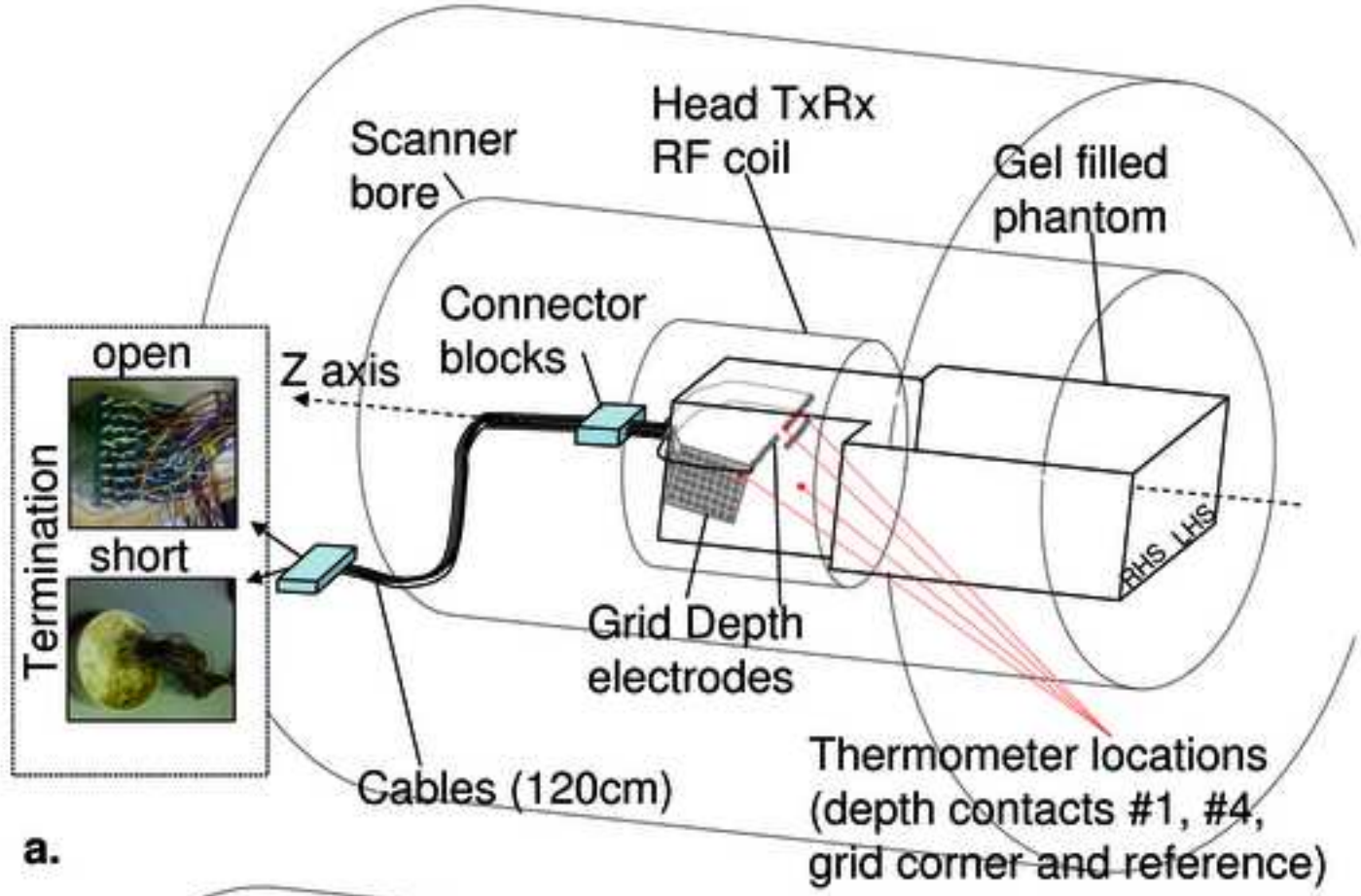

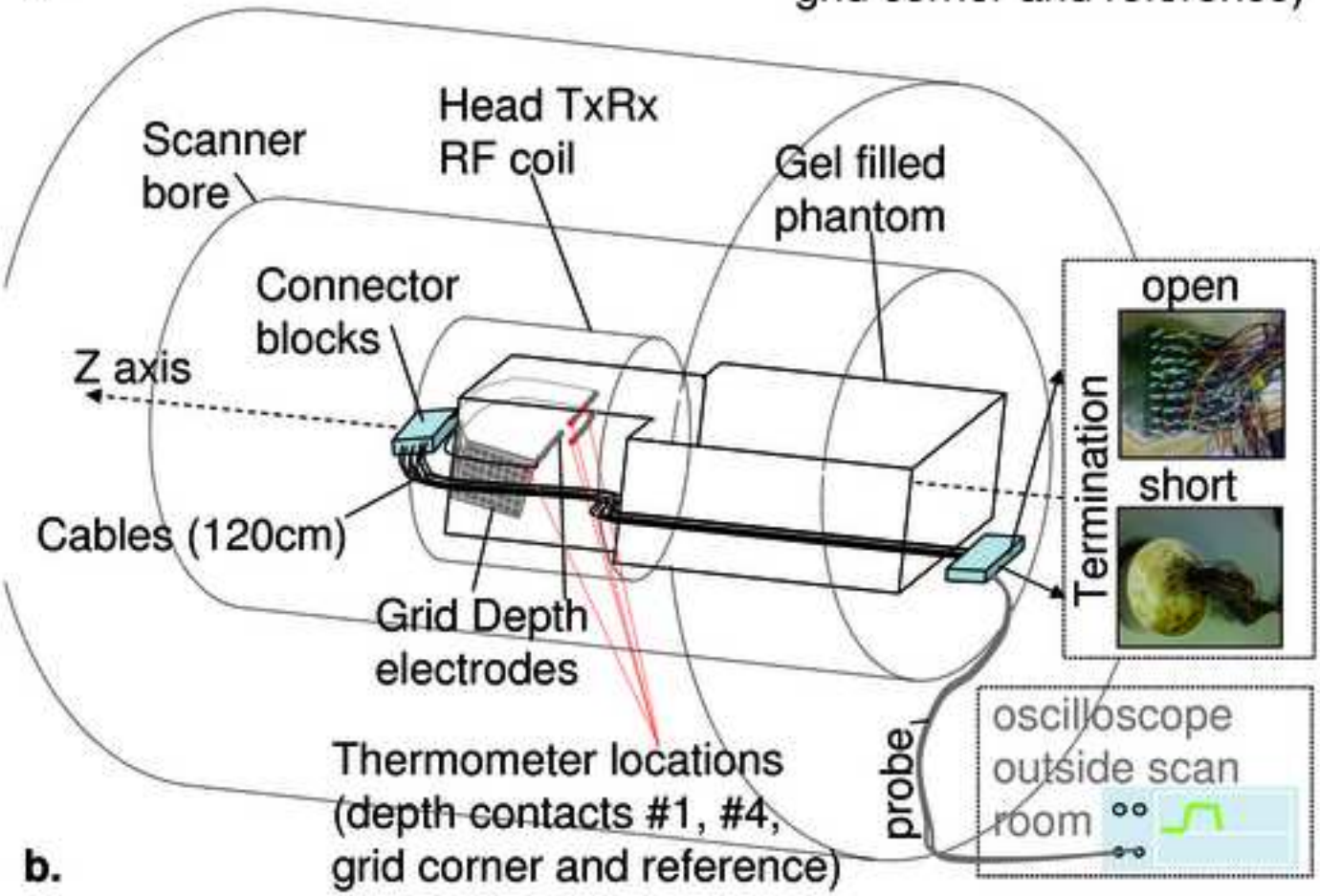

Figure 3

Click here to download high resolution image

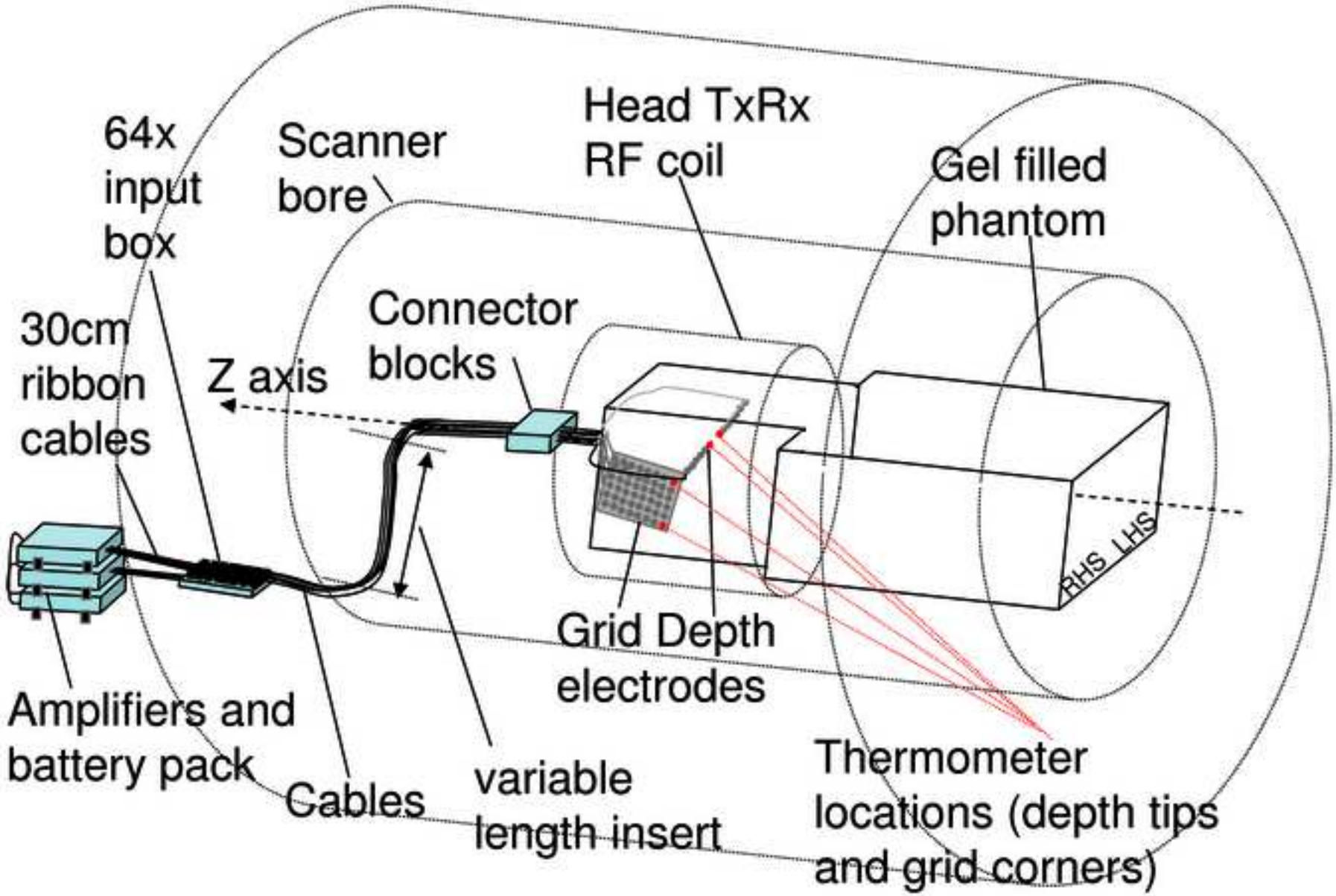

Figure 4

Click here to download high resolution image

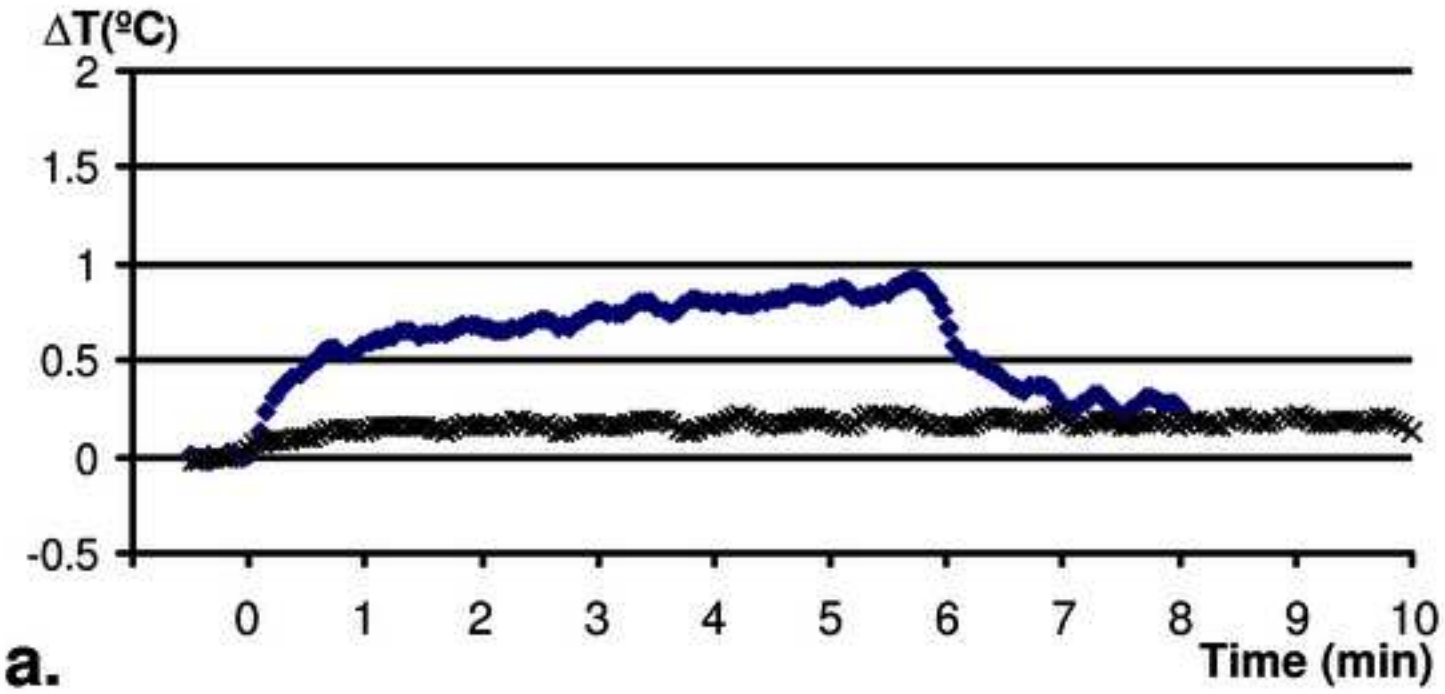

a.

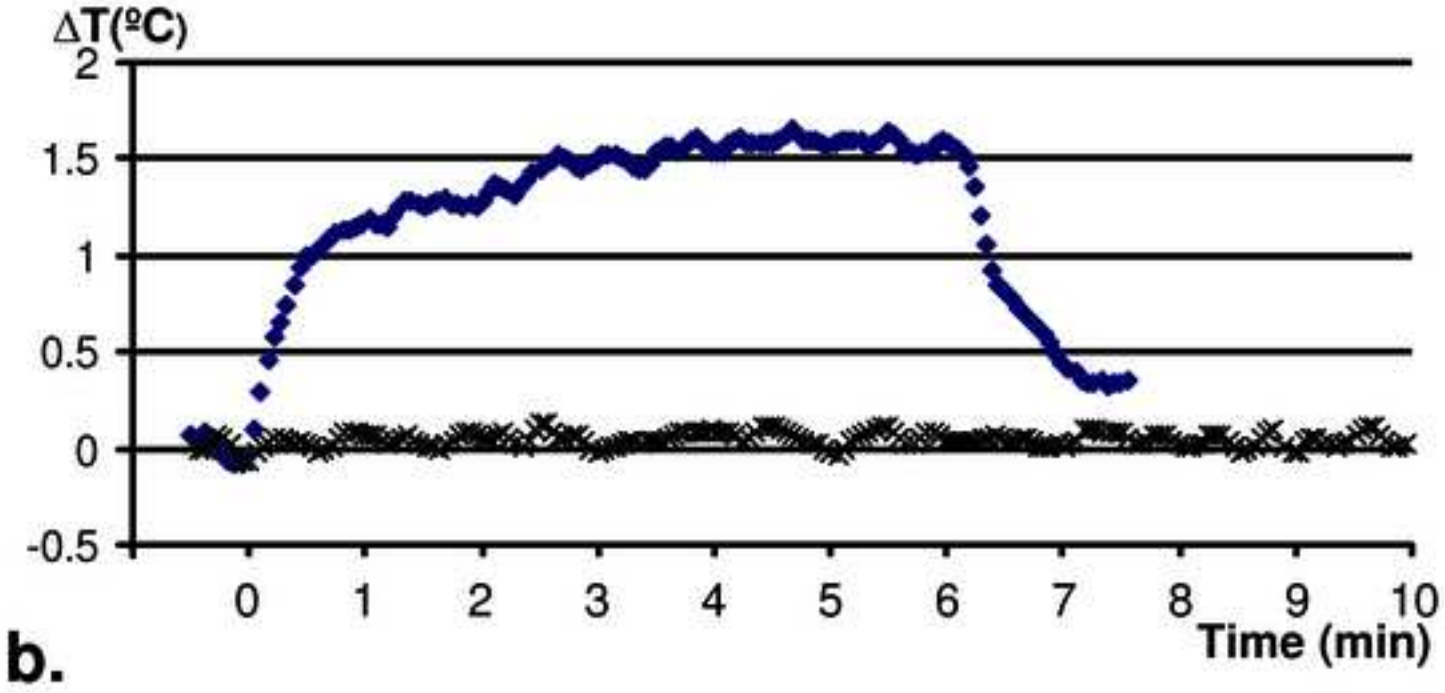

b.

Figure 5

Click here to download high resolution image